Accepted Manuscript

A *Plasmodium falciparum* S33 proline aminopeptidase is associated with changes in erythrocyte deformability

Fabio L. da Silva, Matthew W.A. Dixon, Colin M. Stack, Franka Teuscher, Elena Taran, Malcolm K. Jones, Erica Lovas, Leann Tilley, Christopher L. Brown, Katharine R. Trenholme, John P. Dalton, Donald L. Gardiner, Tina S. Skinner-Adams

PII: S0014-4894(16)30135-7

DOI: 10.1016/j.exppara.2016.06.013

Reference: YEXPR 7268

To appear in: *Experimental Parasitology*

Received Date: 4 April 2016

Revised Date: 22 June 2016

Accepted Date: 29 June 2016

Please cite this article as: da Silva, F.L., Dixon, M.W.A., Stack, C.M., Teuscher, F., Taran, E., Jones, M.K., Lovas, E., Tilley, L., Brown, C.L., Trenholme, K.R., Dalton, J.P., Gardiner, D.L., Skinner-Adams, T.S., A *Plasmodium falciparum* S33 proline aminopeptidase is associated with changes in erythrocyte deformability, *Experimental Parasitology* (2016), doi: 10.1016/j.exppara.2016.06.013.

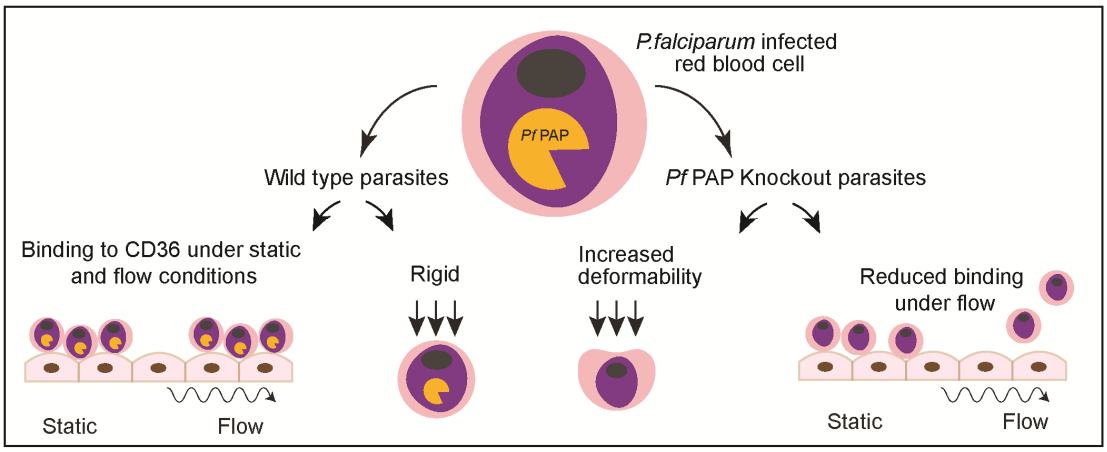
P.falciparum infected red blood cell
Pf PAP
Wild type parasites
Pf PAP Knockout parasites
Binding to CD36 under static and flow conditions
Rigid
Increased deformability
Reduced binding under flow
Static
Flow
Static
Flow

A *Plasmodium falciparum* S33 proline aminopeptidase is associated with changes in erythrocyte deformability

Fabio L. da Silva[a,b,‘ ¶], Matthew WA Dixon[c¶], Colin M. Stack[d¶], Franka Teuscher[b], Elena Taran[e,f], Malcolm K. Jones[g], Erica Lovas[g\], Leann Tilley[c], Christopher L Brown[h,i], Katharine R. Trenholme[b,j], John P. Dalton[a,k], Donald L. Gardiner [b,i] and Tina S. Skinner-Adams[h,i*]

[a]Institute of Parasitology, McGill University, Canada

[b]QIMR Berghofer Medical Research Institute, Australia

[c]Department of Biochemistry and Molecular Biology, Bio21 Institute, and ARC Centre of Excellence for Coherent X-Ray Science, University of Melbourne, Australia

[d]School of Science and Health, University of Western Sydney, Australia

[e]Australian Institute for Bioengineering & Nanotechnology, University of Queensland, Australia

[f]The Australian National Fabrication Facility, Queensland Node, Brisbane, Australia

[g]School of Veterinary Sciences, University of Queensland, Australia

[h]School of Natural Sciences, Griffith University. Brisbane, Queensland 4111, Australia

[i]Eskitis Institute for Drug Discovery, Griffith University, Queensland, Australia

[j] School of Medicine. University of Queensland, Australia

[k]School of Biological Sciences, Queen’s University Belfast, Northern Ireland.

*Corresponding author

Eskitis Institute for Drug Discovery, Griffith University, 46 Don Young Rd Nathan, Queensland, Australia; Tel: 61 37354417; E-mail: t.skinner-adams@griffith.edu.au (TS. Skinner-Adams)

25 ˋPresent address, Fabio L. da Silva

26 Institute of Biology Valrose, Université de Nice-Sophia, F-06108 Nice, France

27

28 ˋPresent address, Erica Lovas

29 Centre for Microscopy & Microanalysis, University of Queensland, Australia

30

31 ¶ These authors contributed equally to this work

32

Abstract

Infection with the apicomplexan parasite *Plasmodium falciparum* is a major cause of morbidity and mortality worldwide. One of the striking features of this parasite is its ability to remodel and decrease the deformability of host red blood cells, a process that contributes to disease. To further understand the virulence of *Pf* we investigated the biochemistry and function of a putative *Pf* S33 proline aminopeptidase (*Pf*PAP). Unlike other *P. falciparum* aminopeptidases, *Pf*PAP contains a predicted protein export element that is non-syntenic with other human infecting *Plasmodium* species. Characterization of *Pf*PAP demonstrated that it is exported into the host red blood cell and that it is a prolyl aminopeptidase with a preference for N-terminal proline substrates. In addition genetic deletion of this exopeptidase was shown to lead to an increase in the deformability of parasite-infected red cells and in reduced adherence to the endothelial cell receptor CD36 under flow conditions. Our studies suggest that *Pf*PAP plays a role in the rigidification and adhesion of infected red blood cells to endothelial surface receptors, a role that may make this protein a novel target for anti-disease interventions strategies.

Index Key Words: prolyl aminopeptidase; malaria; *Plasmodium falciparum;* erythrocyte deformability; cytoadherence

1. Introduction

Parasites of the genus *Plasmodium* are the causative agents of malaria, man's most lethal parasitic disease. The World Health Organization estimates there were approximately 200 million clinical cases and 440,000 deaths due to malaria in 2015 (World Health Organization, 2015). While six *Plasmodium* species can infect humans, *Plasmodium falciparum* (*Pf)* is responsible for the majority of the morbidity and mortality of this disease (World Health Organization, 2015). The virulence of *Pf* malaria, while multi-faceted and not completely understood, is known to be associated with this parasite's ability to mediate the adherence of infected host red blood cells (RBCs) to the endothelium of micro-capillaries causing obstruction and preventing splenic clearance (Miller et al., 2002; Watermeyer et al., 2016). In essence *Pf* remodels host RBCs to facilitate endothelium adherence (reviewed in (Maier et al., 2009)). Remodeling involves the transport and deposition of exported parasite proteins including *Pf* erythrocyte membrane protein (*Pf*EMP) 1 and knob-associated histidine-rich protein (KAHRP) to the host cell membrane (Maier et al., 2009; Watermeyer et al., 2016). RBC cytoskeletal modifications also occur (Cyrklaff et al., 2011; Shi et al., 2013). These host RBC modifications result in changes to RBC surface topology, membrane fluidity, permeability, adhesiveness and deformability (Aikawa, 1997; Atkinson and Aikawa, 1990; Cooke et al., 2004; Glenister et al., 2002; Maier et al., 2009; Nash et al., 1989; Watermeyer et al., 2016). However, the mechanisms driving all of these modifications remain unclear.

To further understand *Pf* mediated RBC remodeling and the virulence of *Pf* we have investigated the biochemistry and function of a putative S33 proline aminopeptidase (*Pf*PAP). Unlike other plasmodial aminopeptidases (www.plasmodb.org) (Schoenen et al., 2010), *Pf*PAP contains a predicted protein export element (PEXEL) (Marti et al., 2004) with the pentameric consensus sequence RILCD which is involved in facilitating the transport of parasite proteins into the host RBC. It is also non-syntenic with other human infecting *Plasmodium* species, suggesting a function unique to *Pf*

(www.plasmodb.org). While little is known about the biology and biochemical characteristics of S33 prolyl aminopeptidases (PAPs), they specifically release amino-terminal proline residues from peptides and are present in a variety of organisms/cells, including fungi (Bolumar et al., 2003), bacteria (Yoshimoto et al., 1999), plants (Waters and Dalling, 1983) and bovine kidney (Khilji et al., 1979). In addition they have been reported to act as virulence factors in some fungi which appear to use this exopeptidase to degrade proline-rich host proteins, such as collagen (Felipe et al., 2005). *Pf*PAP is a 473 amino acid protein characterized by an alpha/beta-hydrolase signature domain (aa 139-449) and an abhydrolase_1 alpha/beta hydrolase fold (aa 195-275). It also contains a PAP motif (aa 140-286), including the catalytic triad (S249, D402, H430) common to serine exopeptidase aminopeptidases. It is encoded by PF3D7_1401300, a two exon gene, with a predicted mRNA sequence of 1422 bp. Interestingly, PF3D7_1401300 is located on the left arm of chromosome 14 (www.plasmodb.org), in a region containing other genes whose protein products are exported into the RBC (Kyes et al., 1999).

2. Materials and Methods

2.1 *In silico* modeling

The protein sequence of *Pf*PAP was retrieved from PlasmoDB (www.plasmodb.org) using the gene ID PF3D7_1401300; a putative aminopeptidase. The sequence was aligned against a validated PAP from *Serratia marcescens*, PDB code 1QTR (Yoshimoto et al., 1999) using ClustalX (Larkin et al., 2007). No similarity was identified for the N-terminal PEXEL region of PF3D7_1401300 so this region was omitted to simplify the homology alignment and modelling process as well as to accelerate molecular dynamics simulations. A preliminary theoretical structural model of the protein was obtained by submission of the PEXEL truncated PF3D7_1401300 protein sequence to SwissModel, a fully automated protein structure homology-modelling server (http://swissmodel.expasy.org/). The initial structural refinement obtained automatically from within the SwissModel system was followed by a

comprehensive explicit solvent molecular dynamics simulation using periodic boundary water solvation and Particle mesh Ewald periodic electrostatic potentials for a total of 2 ns at 310 K, using the free parallel molecular dynamics code NAMD - a program designed and optimized for the high performance simulation of large biomolecular systems (Phillips et al., 2005).

2.2 Recombinant *Pf*PAP

Functional expression of *Pf*PAP was achieved using a truncated form of the enzyme lacking the PEXELated N-terminal Asn-rich repeat region (aa 1-92). This truncated coding sequence was chemically synthesized by GenScript (NJ, USA) using codons optimized for expression in *Eschericia coli* from the PlasmoDB annotated mRNA sequence (for PF3D7_1401300). The gene was cloned into the pTrcHis2B expression vector (Invitrogen, USA) and the construct verified by sequencing before transforming into Rosetta 2 BL21 cells. The cells were grown in 2YT media up to an OD of 0.6 and protein expression induced with 1 mM Isopropyl β-D-1-thiogalactopyranoside (IPTG) for 3 h at 30°C. Cells were lysed in 50 mM TrisHCl pH 7.5 containing 150 mM NaCl and 10 mM imidazole and extracted and solubilized with lysozyme and sonication. Hexa-histidine tagged recombinant *Pf*PAP was purified on a Ni-NTA-agarose column as previously described (Stack et al., 2007).

2.3 Enzymatic analysis

Recombinant *Pf*PAP activity and substrate specificity were determined by measuring the release of the fluorogenic leaving group, 7-amino-4methyl-coumarin (NHMec) from the peptide substrate H-Pro-NHMec. Reactions were carried out in 96-well microtiter plates (100 µl total volume, 30 min, 37°C) using a multi-detection plate reader (BMG LABTECH FLUOstar OPTIMA) with excitation at 370 nm and emission at 460 nm. Initial rates were obtained over a range of substrate concentrations (1-2000 µM) and at fixed enzyme concentration in 50 mM TrisHCl, pH 7.5. The pH

122 profile for recombinant *Pf*PAP was determined from the initial rates of H-Pro-NHMec hydrolysis
123 carried out in constant ionic strength (I = 0.1 M) with acetate/Phosphate/Tris buffers, pH (5-10).
124 Recombinant *Pf*PAP activity against the substrates H-Ala-NHMec, H-Leu-NHMec and H-Glu-NHMec
125 was also examined.
126

127 **2.4 Antibody production**

128 Antibodies to recombinant *Pf*PAP were generated in Balb/c and C57/B6 mice by intraperitoneal
129 injection of 50 μg of purified recombinant protein per mouse in 50 μl PBS mixed with an equal volume
130 of complete Freund's adjuvant. This was followed by a further two immunizations at two week
131 intervals with 50 μg recombinant protein in 50 μl PBS and an equal volume of incomplete Freund's
132 adjuvant. Two weeks after the last injection test bleeds were performed and antibody titers to the
133 recombinant protein measured by enzyme linked immuno-sorbent assay. Mice were then euthanized
134 and blood collected by cardiac puncture.
135

136 **2.5 Parasites**

137 The *Pf* parasite clones 3D7 and D10 were cultured *in vitro* in Roswell Park Memorial Institute
138 (RPMI) medium supplemented with 10% human serum as previously described (Trager and Jensen,
139 1976). RBCs and pooled serum were obtained from the Red Cross Transfusion Service (Brisbane,
140 QLD, Australia). *Pf*3D7 is a cytoadherent *Pf* clone possessing a complete chromosome 9, while D10 is
141 a non cytoadherent *Pf* clone lacking the right arm of chromosome 9.
142

143 **2.6 Northern blotting**

144 Northern blotting was performed with total RNA extracts prepared using TRIzol (Invitrogen) as
145 previously described (Kyes et al., 2000). Blots were probed with a purified 1504 bp PCR fragment

corresponding to the full length genomic copy of *Pf*PAP amplified from genomic *Pf* DNA using primers PAPF (ATGAGAAATATTAATGGGT) and PAPR (TGTTTTATATTGACCATTTTT). Probes were labelled with [α-^{32}P] dATP by random priming (DECAprime II, Ambion Inc). The probe was hybridized overnight at 40^{o}C in a hybridization buffer containing formamide (Northern Max; Ambion). The filter was washed once at low stringency and twice at high stringency (Northern Max; Ambion), then exposed to film overnight.

2.7 Quantitative real-time PCR

The stage specific expression of *Pf*PAP was examined by reverse transcription-quantitative polymerase chain reaction (RT-qPCR). The *Pf* clonal line 3D7 was synchronized using two rounds of sorbitol treatment (Lambros and Vanderberg, 1979) (>99% early ring stage parasites) and parasites samples harvested at 0, 12, 18, 24, and 36 h. Transcript levels were assessed by extracting total RNA as previously described (Kyes et al., 2000) and generating cDNA (QuantiTect Reverse Transcription Kit, Qiagen). Quantitative PCR was performed using a Rotor-Gene 6000 real time PCR Cycler (Corbett Research/Qiagen, Australia). Briefly cDNA was added to SYBR Green PCR Master-mix (Applied Biosystems, Australia) together with *PfPAP* specific primers (forward TCACCCGTTGGTGTATTGAA and reverse TGGTTACCACCATTCCCAAT) or internal reference primers (*18s rRNA;* PF3D7_0725600, forward CGGCGAGTACACTATATTCTTA and reverse TTAGTAGAACAGGGAAAAGGAT (Augagneur et al., 2012) or *Seryl-tRNA synthetase*, PF3D7_0717700, forward ATAGCTACCTCAGAACAACC and reverse CAAGATGAGAATCCAGCGTA (Roseler et al., 2012). Each run was performed in triplicate and repeated twice. Data were analysed with Rotor-Gene 6.0 software with *PfPAP* transcription calculated relative to both reference genes using the standard curve method and presented as mean ± SEM (Corbett Research/Qiagen, Australia).

2.8 Construction of the transgenic expression plasmids and parasites

PF3D7_1401300 was PCR amplified from *Pf* clone D10 genomic DNA using the forward primer PAPBglF (**AGATCT**ATGAGAAATATTAATGGGT; containing a *Bgl*II restriction site, in bold) and the reverse primer PAPPstR (**CTGCAG**TGTTTTATATTGACCATTTTT; containing a *Pst*I restriction site, in bold). The PCR product was cloned into pGEM using a TA cloning system (Promega, USA) and sequenced to confirm that no *Taq*-associated errors had occurred. Full length fragments were digested out of the pGEM vector using *Bgl*II and *Pst*I and subcloned into the previously digested (using *Bgl*II and *Pst*I) Gateway™ (InvitroGen) compatible entry vector pHGFPB . In this vector the introduced gene is ligated in frame with a 3' green florescent protein (GFP)-tag under the control of the heat shock protein 86 promoter (Dixon et al., 2008). This entry vector was designated pHB-PF1401300-GFP. A clonase reaction was then performed using this entry vector and a Gateway™ compatible destination vector with a destination cassette and a second cassette containing the human dihydrofolate reductase synthase gene under the control of the *Pf* calmodulin promoter as a selectable marker (conferring resistance to the anti-folate drug, WR92210). The final plasmid was designated pHH1-PF1401300-GFPB. For transfection, ring stage parasites were subjected to electroporation in the presence of 50 µg of plasmid DNA as described (Wu et al., 1995). Parasites resistant to WR99210 were obtained <25 days later.

2.9 Creation of knockout parasite clones

A transfection vector intended to disrupt the *Pf*PAP gene by double homologous recombination was designed using a positive negative selection strategy. This vector had previously undergone extensive modifications for use with the Gateway™ Cloning system. In the original modification the human dihydrofolate reductase synthase gene was used for positive selection and the Herpes simplex

thymidine kinase (*tk*) gene used for negative selection (sensitivity to ganciclovir). However in the current vector the *tk* gene was removed and replaced with the cytosine deaminase gene of *Escherichia coli*. This entry vector was then further modified by the addition of an *Avr*II site 10 bp from the unique *Sal*I site upstream of the heat shock protein 86 promoter, allowing the insertion of the 5′-targeting sequence by directional cloning. The destination vector contained the human dihydrofolate reductase synthase gene under the control of the *Pf* calmodulin promoter and, downstream, the unique *Avr*II/*Cla*I cloning site. The 3′-targeting sequence was inserted into this site via directional cloning. A clonase reaction of the entry and destination vectors produced the final transfection vector (pHH1-*Pf*PAPDKO). Plasmid DNA was generated and transfected into *Pf* 3D7 parasites as previously described. Parasites resistant to WR92210 were detected 30 days post transfection. Parasites were cycled on both WR99210 and 5-fluoro-uracil until integration of the vector into the genomic copy of the *Pf*PAP gene was detected by PCR. These cultures were cloned by limiting dilution.

The pHH1-*Pf*PAPDKO transfection vector contained a 5`-targeting sequence generated by PCR amplification of DNA from *Pf* clone 3D7 using the primers PAPDKO5F (**CCTAGG**CTTAAGTACATATGATAAACT) and PAPDKO5R (**GTCGAC**AGGTTCAAATG CTTTAATAAT). Restriction endonuclease sites are listed in bold. This generated a 739 bp fragment that was cloned into a pGEM Teasy vector (Promega), and sequenced. Digestion of this vector with the appropriate restriction endonucleases allowed directional cloning of the fragment into the entry vector. For the 3` targeting sequence a 641 bp PCR fragment was generated using the primers PAPDKO3F (**ATCGAT**TGGG ATGTATAATAGCCGCAG) and PAPDKO3R (**CCTAGG**TTA-TCAATAGTAATCTGTTT). This PCR fragment was cloned into a pGEM Teasy vector (Promega), and sequenced to confirm the sequence. Digestion of this vector with the appropriate restriction endonucleases allowed directional cloning of the fragment into the destination vector.

2.10 Western Blotting

After washing infected RBCs in phosphate-buffered saline (PBS), parasites were released by incubation with 0.03% saponin in PBS at 4°C. Resulting parasite pellets were washed three times with PBS then lysed in distilled H_2O for 2 min, followed by centrifugation at 14,000 g. Parasite supernatants were stored at 4°C. Proteins of saponin-lysed parasite extracts were resolved on reducing 10% SDS-PAGE gels, transferred to a nitrocellulose membrane and probed with the anti-*Pf*PAP antisera (1:250 dilution) followed by a horseradish peroxidase-labelled anti-mouse IgG antibody (1:5000 dilution, Chemicon International Inc.). The membrane was stripped and re-probed with an anti-glyceraldehyde-3-phosphate-dehydrogenase (GAPDH) rabbit antibody (1:5000 dilution) to demonstrate transfer of malaria proteins (Spielmann et al., 2006).

2.11 Fluorescence Microscopy

Fluorescence and phase contrast images were collected with an Axioscope 2 Mot + (Zeiss) equipped with a Zeiss 63x/1.4 Plan Apochromat lens. Live parasites were mounted in PBS and observed at ambient temperature. Parasite DNA was visualized by adding Hoechst dye (0.5 µg/ml) and incubating at 37°C for 10 min prior to mounting. For indirect fluorescence, concanavalin A (0.5 mg/ml) was added to each well of a multi-well slide and incubated for 30 min at 37°C after which infected RBCs were added, incubated at room temperature for 15 min and unbound cells removed by washing with PBS. The cells were fixed in 4% formaldehyde/0.005% glutaraldehyde and probed with anti-*Pf*PAP anti-serum or with a mouse monoclonal antibody to GFP (diluted 1:500). Bound antibody was visualized with goat anti-mouse Ig-Cy2 (10 µg/ml). Immunofluorescence assays for the detection of KAHRP, Ring-exported protein-1 (REX1), and *Pf*EMP-3 were performed as previously described (Dixon et al., 2008). Briefly, thin blood smears of trophozoite stage parasites were made for both parent and *Pf*PAP knockout (PAPKO) cells, air dried and fixed in cold acetone for 10 min. Slides were

washed in 1X PBS and all antibody incubations were performed in 3% BSA 1X PBS for 1 h at room temperature. The following primary antibodies were used: anti-KAHRP mouse (1:500), anti-*Pf*EMP-3 mouse (1:500) and anti-REX1 rabbit (1:2000). Slides were washed three times in 1X PBS prior to addition of anti-rabbit FITC and anti-mouse Alexa Fluor 647. Secondary antibodies were washed from the slides and the nuclei stained with 10 µg/ml of 4',6-diamidino-2-phenylindole (DAPI) prior to mounting of slides. Images were taken on a Delta Vision (DV) Elite Microscope with 100X oil objective. Images were processed using NIH ImageJ version 1.48c (http://imagej.nih.gov/ij/).

2.12 Atomic force microscopy

To investigate the mechanical properties of the infected and uninfected RBCs, arrays of 20 x 20 force curves on a 10 x10 µm area were recorded on samples immersed in PBS employing an MFP-3D (Asylum Research) atomic force microscope (AFM) in force spectroscopy mode. The AFM was mounted on an anti-vibrational table (Herzan) and operated within an acoustic isolation enclosure (TMC, USA). The force curves were recorded using a SiNi cantilever (Budget Sensors, Bulgaria) having a nominal spring constant K_N = 0.06 N/m. Prior to use the cantilevers had been calibrated against a glass slide, using the thermal vibration method embedded in the AFM processing software. All experiments were repeated 4 times in triplicate with the loading force kept constant at 20 nN and the velocity at 1 µm/s. Force curve data were analysed using IGOR software. The Young's modulus, E, (± SD) was calculated using the Hertz model.

2.13 Spleen mimic filtration

Parent 3D7 and 3D7-PAPKO parasites were synchronized to a 2 h window (Lambros and Vanderberg, 1979). Spleen mimic filtration was performed as previously described (Deplaine et al., 2011). Briefly, parasite infected RBCs at 5% parasitemia were re-suspended at 1% hematocrit in 1%

AlbuMax II in PBS. The solution was flowed over a 5 mm bead volume of calibrated metal microbeads ranging in size from 5-25 μm at a rate of 60 ml/h. The percentage parasitaemia pre and post filtration was assessed via Giemsa stained thin blood films and used to calculate the percentage of parasites present in the flow through (% flow). Three biological repeats were performed.

2.14 Cytoadherence assays

Cytoadherence assays were performed using prefabricated slides (ibidi GmbH). Slides were coated with 125 μg/ml of recombinant CD36 in PBS overnight prior to blocking with 1% BSA for 1 h at 37^{o}C. The slides were washed with RPMI-HEPES (minus $NaHCO_3$). All assays were performed on a DV elite microscope with environmental chamber set at 37^{o}C.

Parasite infected RBCs at 3% parasitemia and 1% haematocrit in RPMI-HEPES (minus $NaHCO_3$) were flowed through the chamber for 5 min at a pressure of 0.1 or 0.05 Pa prior to a further washing (5 min) with RPMI-HEPES (minus $NaHCO_3$). Washing and counting was performed under the same conditions as binding. The number of parasite infected RBCs bound in 20 fields were counted, and expressed as parasites bound per mm^2 (Crabb et al., 1997). Three biological repeats were performed.

2.15 Electron microscopy

Parasite infected RBCs were embedded in 1% molten agarose in 0.1 M phosphate buffer. The agarose blocks were processed into Epon resin using a Pelco 34700 Biowave Microwave Oven (Ted Pella Inc., Redding, CA). Cells were post-fixed in aqueous potassium ferricyanide-reduced osmium tetroxide and dehydrated in ethanol prior to infiltration and embedment in Epon resin. Unstained ultrathin sections were observed and photographed using a JEOL 1011 transmission electron

289 microscope (JEOL Ltd, Tokyo, Japan) equipped with an Olympus Morada side-mounted digital camera
290 (Olympus, USA).
291
292 **3. Results**
293 **3.1 *In silico* modeling of *Pf*PAP**
294 While no malaria parasite PAP structures currently exist in the protein data bank (PDB), X-ray
295 derived solid-state structures of several other validated PAPs have been determined
296 (http://www.rcsb.org (Berman et al., 2000)). To provide additional evidence that *Pf*PAP is indeed a
297 PAP its amino acid sequence was aligned with a validated PAP derived from *Serratia marcescens*
298 (Yoshimoto et al., 1999) (PDB code 1QTR; Fig 1, panels A, B and C; 41% similarity with *Pf*PAP; with
299 specific N-terminal PEXEL sequence removed). Co-alignment of catalytically significant triad residues
300 (Ser249, Asp402, His430) and other highly conserved residues, characteristic of PAPs, provided further
301 evidence that *Pf*PAP belongs to this class of protein (Fig 1A). The primary sequence similarity
302 observed in the alignment was also observed in the structural homology model. Comparison of the
303 *Pf*PAP structural model with the X-ray derived structure of *S. marcescens* PAP (PDB code 1QTR)
304 revealed that the spatial distributions of catalytic residues and other notable residues (Fig 1C) are
305 highly conserved, further supporting the proposed function of PF3D7_1401300.
306
307 **3.2 Biochemical characterization of functionally active recombinant *Pf*PAP**
308 *Pf*PAP was expressed and purified as a recombinant protein (r*Pf*PAP) from bacterial cells. The
309 enzyme resolved as a single protein of ~45 kDa (Fig 2A) and immunoblotting confirmed expression of
310 the recombinant protein (Fig 2B). Using the fluorogenic substrate H-Pro-NHMec (7-amido-4-
311 methylcoumarin), r*Pf*PAP exhibited a Km of 403 μM and a Kcat/Km value 28.28 M^{-1} s^{-1} (Fig 2C).
312 Experiments investigating the specificity of r*Pf*PAP demonstrate a low, but significant, level of activity

when incubated with the fluorogenic substrate H-Ala-NHMec (2-5% compared to H-Pro-NHMec) but no hydrolysis of H-Leu-NHMec or H-Glu-NHMec. When the metal chelator *o*-phenanthroline (2 mM) was added, only slight inhibition of r*Pf*PAP activity was observed, confirming the activity is specific and not due to contaminating bacterial neutral aminopeptidases (not shown).

3.3 *Pf*PAP is transcribed throughout the intraerythrocytic asexual lifecycle and exported into the host RBC

Northern blot analysis indicated that *Pf* transcribes a single species of mRNA with an apparent size of ~3 kbp throughout the intraerythrocytic life cycle (Fig 3A). Quantitative analysis of transcription suggested that peak expression occurs early in development (Fig 3B).

Western blot analysis of parent 3D7 parasites with anti-*Pf*PAP antiserum revealed a single species with an apparent molecular weight (MW) of ~40 kDa (Fig 3C). Immunochemistry using an anti-GFP antibody on a transgenic GFP-tagged *Pf*PAP chimeric protein also identified a single protein species (not shown). Immunofluorescence analysis using anti-*Pf*PAP antibody localized *Pf*PAP to the infected RBC cytoplasm which was confirmed in GFP-tagged *Pf*PAP transfected parasites (Fig 3D).

3.4 Targeted gene disruption (TGD) of *Pf*PAP changes the viscoelastic properties of the infected RBC membrane

PCR analysis indicated that a single homologous recombination of the 5` targeting sequence had occurred in the clone selected for further study. Nonetheless this led to a truncation of the genomic copy and Western blot analysis using antibodies to r*Pf*PAP indicated loss of *Pf*PAP expression (Fig 3C).

Genetic disruption of PF3D7_1401300 caused no obvious changes in macroscopic phenotype, including life cycle length, or in parasite viability *in vitro*. However, significant changes in the

viscoelastic properties of the infected RBC plasma membrane were observed using AFM. The Young's modulus value (E) was determined to be 760 ± 140 kPa for uninfected RBCs, and 1760 ± 710 kPa for 3D7 early trophozoite infected RBCs. However, 3D7_PAP-KO early trophozoite –infected RBCs generated a Young's modulus value of 800 ± 250 kPa. .

A microbead filtration system that mimics the splenic microcirculation was employed to assess RBC deformability changes in more detail (Fig 4A). Tightly synchronized parasites were analyzed 16, 18, 20 and 26 h post invasion. No significant difference between the percentage of 3D7 and 3D7_PAP-KO parasites in the flow through was seen at 16 h (64 ± 14% vs 58 ± 6%; relative to starting parasitemia). However, 3D7_PAP-KO parasites were significantly more filterable than 3D7 parasites at 18 to 26 h post-invasion (18 h: 64 ± 4% vs 41 ± 5%; 20 h: 58 ± 6% vs 26 ± 3%; and 26 h: 40 ± 5% vs 21 + 3%; P = 0.0001) (Fig 4A).

The impact of *Pf*PAP TGD on the expression and transport of proteins thought to play a role in the trafficking of unique *Pf* cytoadherence proteins, such as *Pf*EMP-1, to the infected RBC surface was assessed. Data demonstrated that TGD of *Pf*PAP does not change the location of KAHRP, ring-exported protein-1 (REX1), skeleton-binding protein-1 (SBP1) or *Pf*EMP-3. Each of these proteins was found at the RBC membrane or Maurer's clefts of 3D7 and 3D7PAPKO parasites (Fig 4B). Electron microscopy also confirmed the presence of electron dense structures at the infected RBC plasma membrane of both 3D7 (not shown) and 3D7PAPKO parasites (Fig 4C), consistent with correct trafficking and delivery of KAHRP.

The presence of *Pf*EMP-1 at the surface of both 3D7 and 3D7PAPKO parasites was demonstrated by trypsin cleavage (Fig 5A). Cleavage products (75-100 kDa) were observed in trypsin-treated (T) samples but were absent from samples with no trypsin (P) or with trypsin plus inhibitor (i) (Fig 5A). Consistent with these data parent 3D7 and 3D7_PAP-KO infected RBCs adhered to recombinant CD36 at similar levels under static conditions (Fig 5B). However, assessment of binding

under physiological flow conditions demonstrated that 3D7 infected RBCs bound at 500 ± 20 infected RBC/mm^2 while the 3D7_PAP-KO infected RBCs bound at a significantly lower rate (367 ± 16 infected RBC/mm^2; $P < 0.0001$). This significant decrease in binding was also seen at the higher shear stress of 0.1 Pa. (Fig 5C).

4. Discussion

In this work PF3D7_1401300-encoded *Pf*PAP was verified as an aminopeptidase with a preference for N-terminal proline substrates and with a weaker specificity for substrates containing N-terminal alanine. While the fine specificities of various S33 clan members can vary, a weak specificity for N-terminal alanine is not uncommon in this group of enzymes. PAPs are not obligate proline aminopeptidases, with members being capable of cleaving additional residues including alanine (Mahon et al., 2009). A sequence comparison of *Pf*PAP with the well described PAP protein from *Serratia marcescens* (PDB code 1QTR) (Fig 1, panels A, B and C) also demonstrated the conserved location of catalytic triad residues in *Pf*PAP.

Particularly interesting features of *Pf*PAP are that it is unique to *Pf* and contains a protein export element (PEXEL) or vacuolar transit sequence (VTS) (www.plasmo.db.org). The presence of an export sequence suggests that unlike all other characterised *Pf* aminopeptidases, this enzyme is transported into the RBC cytoplasm. One of the important functions of exported proteins is to modify the host RBC membrane to facilitate adhesion to blood vessel walls, an event that underlies much of the pathophysiology of *Pf* infections. For example a number of exported parasite proteins facilitate the presentation of the adhesin, *Pf*EMP-1, at the RBC surface. They achieve this by reorganizing the host RBC membrane skeleton and by forming raised structures, known as knobs. The surface presentation of *Pf*EMP-1 at the knobby protrusions facilitates binding to endothelial receptors, such as CD36 (Crabb et al., 1997). Intra-erythrocytic maturation of *Pf* is also associated with RBC membrane rigidification

385 (Glenister et al., 2002). While KAHRP and *Pf*EMP-3 are responsible for about 50% of the observed
386 rigidification (Glenister et al., 2002), it is recognized that other structural proteins and enzymes can
387 contribute to the reorganization of the membrane skeleton and rigidification (Glenister et al., 2002;
388 Sanyal et al., 2012).

389 To investigate the role of *Pf*PAP in RBC re-modelling and cytoadherence we examined the
390 expression and location of *Pf*PAP within infected RBCs. We also performed a TGD of *Pf*PAP. In these
391 studies the expression of *Pf*EMP-1, REX1, KAHRP and *Pf*EMP-3 was examined as was host RBC
392 rigidity, deformability and CD36-mediated cytoadherence. Our data demonstrated that *Pf*PAP is
393 exported into the host RBC cytoplasm (Fig 3D) and that it is highly expressed early in the parasite
394 asexual intra-erythrocytic life cycle (Fig 3B), characteristics that support a role in RBC remodeling.
395 They also showed that while static CD36-mediated adhesion is not changed by *Pf*PAPKO, adherence is
396 weaker under flow conditions (Fig 5). In addition the rigidity and filterability (Fig 4) of host RBCs
397 infected with parasites no longer able to express *Pf*PAP is reduced when compared to wild-type
398 parasites. Interestingly TGD of *Pf*PAP had no impact on the delivery of KAHRP or *Pf*EMP-3 to the
399 RBC membrane skeleton (Fig 4). It also had no impact on the delivery of REX1 or *Pf*EMP-1 to their
400 known locations in the Maurer's clefts and RBC surface respectively (Figs 4 and 5).

401 While the precise role of the *Pf*PAP remains to be elucidated, current data suggest that this
402 protein plays a role in host RBC re-modelling independent of *Pf*EMP-1, *Pf*EMP-3, KAHRP and REX1
403 and that this role results in reduced RBC rigidity and cytoadherence under flow conditions. These data
404 fit well with the non-essential nature of *Pf*PAP *in vitro* where parasites are not dependent on
405 cytoadherence and RBC deformability to survive. The ability of parasites to cytoadhere and avoid
406 splenic clearance *in vivo* is of no advantage to parasites *in vitro*. Nevertheless, caution must be
407 exercised before drawing firm conclusions in this regard. The current study did not investigate the
408 expression of STEVOR (subtelomeric variant open reading frame) proteins in wild-type and transgenic

409 parasites and recent studies have demonstrated that these proteins play a role in the deformability of
410 host RBCs infected with *Pf* gametocytes and asexual stages (Sanyal et al., 2012; Tiburcio et al., 2012).
411 In addition, while the *Pf*EMP-1 variant expressed by both wild-type and *Pf*PAPKO parasites in this
412 study demonstrated a comparable preference for CD36 under static conditions (Fig 5) further studies
413 examining the impact of these variant proteins on RBC deformability and adherence under shear flow
414 conditions were not performed, however care was taken to ensure that CD36 specific *Pf*EMP-1 binding
415 variants were expressed by panning of parasites to CD36.

416 The current study verified PF3D7_1401300-encoded *Pf*PAP as a PAP and has provided the first
417 insights into the functional role of this exported protease. Although further work including the analysis
418 of additional clones, an assessment of expressed *stevor* genes in clones and an assessment of the impact
419 of *var* gene expression on this protein's apparent role in RBC re-modelling is required to fully elucidate
420 the role of *Pf*PAP in modifying the host RBC and to determine its contribution to survival fitness *in*
421 *vivo,* the current data suggest that drugs designed to inhibit *Pf*PAP may be useful in preventing
422 sequestration of the asexual stage in the micro-capillaries and warrants further investigation as an anti-
423 disease drug target.

424

Acknowledgements

This work was supported by the National Health & Medical Research Council of Australia and the Australia Research Council (PD0666128).

References

Aikawa, M., 1997. Studies on falciparum malaria with atomic-force and surface-potential microscopes. Ann Trop Med Parasitol 91, 689-692.

Atkinson, C.T., Aikawa, M., 1990. Ultrastructure of malaria-infected erythrocytes. Blood Cells 16, 351-368.

Augagneur, Y., Wesolowski, D., Tae, H.S., Altman, S., Ben Mamoun, C., 2012. Gene selective mRNA cleavage inhibits the development of *Plasmodium falciparum*. Proc Natl Acad Sci U S A 109, 6235-6240.

Berman, H.M., Westbrook, J., Feng, Z., Gilliland, G., Bhat, T.N., Weissig, H., Shindyalov, I.N., Bourne, P.E., 2000. The Protein Data Bank. Nucleic Acids Res 28, 235-242.

Bolumar, T., Sanz, Y., Aristoy, M.C., Toldra, F., 2003. Purification and characterization of a prolyl aminopeptidase from *Debaryomyces hansenii*. Appl Environ Microbiol 69, 227-232.

Cooke, B.M., Mohandas, N., Coppel, R.L., 2004. Malaria and the red blood cell membrane. Semin Hematol 41, 173-188.

443 Crabb, B.S., Cooke, B.M., Reeder, J.C., Waller, R.F., Caruana, S.R., Davern, K.M., Wickham, M.E.,
444 Brown, G.V., Coppel, R.L., Cowman, A.F., 1997. Targeted gene disruption shows that knobs enable
445 malaria-infected red cells to cytoadhere under physiological shear stress. Cell 89, 287-296.

446 Cyrklaff, M., Sanchez, C.P., Kilian, N., Bisseye, C., Simpore, J., Frischknecht, F., Lanzer, M., 2011.
447 Hemoglobins S and C interfere with actin remodeling in *Plasmodium falciparum*-infected erythrocytes.
448 Science 334, 1283-1286.

449 Deplaine, G., Safeukui, I., Jeddi, F., Lacoste, F., Brousse, V., Perrot, S., Biligui, S., Guillotte, M.,
450 Guitton, C., Dokmak, S., Aussilhou, B., Sauvanet, A., Cazals Hatem, D., Paye, F., Thellier, M., Mazier,
451 D., Milon, G., Mohandas, N., Mercereau-Puijalon, O., David, P.H., Buffet, P.A., 2011. The sensing of
452 poorly deformable red blood cells by the human spleen can be mimicked *in vitro*. Blood 117, e88-95.

453 Dixon, M.W., Hawthorne, P.L., Spielmann, T., Anderson, K.L., Trenholme, K.R., Gardiner, D.L.,
454 2008. Targeting of the ring exported protein 1 to the Maurer's clefts is mediated by a two-phase
455 process. Traffic 9, 1316-1326.

456 Felipe, M.S., Andrade, R.V., Arraes, F.B., Nicola, A.M., Maranhao, A.Q., Torres, F.A., Silva-Pereira,
457 I., Pocas-Fonseca, M.J., Campos, E.G., Moraes, L.M., Andrade, P.A., Tavares, A.H., Silva, S.S.,
458 Kyaw, C.M., Souza, D.P., Pereira, M., Jesuino, R.S., Andrade, E.V., Parente, J.A., Oliveira, G.S.,
459 Barbosa, M.S., Martins, N.F., Fachin, A.L., Cardoso, R.S., Passos, G.A., Almeida, N.F., Walter, M.E.,
460 Soares, C.M., Carvalho, M.J., Brigido, M.M., PbGenome, N., 2005. Transcriptional profiles of the
461 human pathogenic fungus *Paracoccidioides brasiliensis* in mycelium and yeast cells. J Biol Chem 280,
462 24706-24714.

463 Glenister, F.K., Coppel, R.L., Cowman, A.F., Mohandas, N., Cooke, B.M., 2002. Contribution of
464 parasite proteins to altered mechanical properties of malaria-infected red blood cells. Blood 99, 1060-
465 1063.

466 Khilji, M.A., Akrawi, A.F., Bailey, G.S., 1979. Purification and partial characterisation of a bovine
467 kidney aminotripeptidase (capable of cleaving prolyl-glycylglycine). Mol Cell Biochem 23, 45-52.

468 Kyes, S., Pinches, R., Newbold, C., 2000. A simple RNA analysis method shows var and rif multigene
469 family expression patterns in *Plasmodium falciparum*. Mol Biochem Parasitol 105, 311-315.

470 Kyes, S.A., Rowe, J.A., Kriek, N., Newbold, C.I., 1999. Rifins: a second family of clonally variant
471 proteins expressed on the surface of red cells infected with *Plasmodium falciparum*. Proc Natl Acad Sci
472 U S A 96, 9333-9338.

473 Lambros, C., Vanderberg, J.P., 1979. Synchronization of *Plasmodium falciparum* erythrocytic stages in
474 culture. J Parasitol 65, 418-420.

475 Larkin, M.A., Blackshields, G., Brown, N.P., Chenna, R., McGettigan, P.A., McWilliam, H., Valentin,
476 F., Wallace, I.M., Wilm, A., Lopez, R., Thompson, J.D., Gibson, T.J., Higgins, D.G., 2007. Clustal W
477 and Clustal X version 2.0. Bioinformatics 23, 2947-2948.

478 Mahon, C.S., O'Donoghue, A.J., Goetz, D.H., Murray, P.G., Craik, C.S., Tuohy, M.G., 2009.
479 Characterization of a multimeric, eukaryotic prolyl aminopeptidase: an inducible and highly specific
480 intracellular peptidase from the non-pathogenic fungus *Talaromyces emersonii*. Microbiology 155,
481 3673-3682.

Maier, A.G., Cooke, B.M., Cowman, A.F., Tilley, L., 2009. Malaria parasite proteins that remodel the host erythrocyte. Nat Rev Microbiol 7, 341-354.

Marti, M., Good, R.T., Rug, M., Knuepfer, E., Cowman, A.F., 2004. Targeting malaria virulence and remodeling proteins to the host erythrocyte. Science 306, 1930-1933.

Miller, L.H., Baruch, D.I., Marsh, K., Doumbo, O.K., 2002. The pathogenic basis of malaria. Nature 415, 673-679.

Nash, G.B., O'Brien, E., Gordon-Smith, E.C., Dormandy, J.A., 1989. Abnormalities in the mechanical properties of red blood cells caused by *Plasmodium falciparum*. Blood 74, 855-861.

Phillips, J.C., Braun, R., Wang, W., Gumbart, J., Tajkhorshid, E., Villa, E., Chipot, C., Skeel, R.D., Kale, L., Schulten, K., 2005. Scalable molecular dynamics with NAMD. J Comput Chem 26, 1781-1802.

Roseler, A., Prieto, J.H., Iozef, R., Hecker, B., Schirmer, R.H., Kulzer, S., Przyborski, J., Rahlfs, S., Becker, K., 2012. Insight into the selenoproteome of the malaria parasite *Plasmodium falciparum*. Antioxid Redox Signal 17, 534-543.

Sanyal, S., Egee, S., Bouyer, G., Perrot, S., Safeukui, I., Bischoff, E., Buffet, P., Deitsch, K.W., Mercereau-Puijalon, O., David, P.H., Templeton, T.J., Lavazec, C., 2012. *Plasmodium falciparum* STEVOR proteins impact erythrocyte mechanical properties. Blood 119, e1-8.

499 Schoenen, F.J., Weiner, W.S., Baillargeon, P., Brown, C.L., Chase, P., Ferguson, J., Fernandez-Vega,
500 V., Ghosh, P., Hodder, P., Krise, J.P., Matharu, D.S., Neuenswander, B., Porubsky, P., Rogers, S.,
501 Skinner-Adams, T., Sosa, M., Spicer, T., To, J., Tower, N.A., Trenholme, K.R., Wang, J., Whipple, D.,
502 Aube, J., Rosen, H., White, E.L., Dalton, J.P., Gardiner, D.L., 2010. Inhibitors of the *Plasmodium*
503 *falciparum* M18 Aspartyl Aminopeptidase, Probe Reports from the NIH Molecular Libraries Program,
504 Bethesda (MD).

505 Shi, H., Liu, Z., Li, A., Yin, J., Chong, A.G., Tan, K.S., Zhang, Y., Lim, C.T., 2013. Life cycle-
506 dependent cytoskeletal modifications in *Plasmodium falciparum* infected erythrocytes. PLoS One 8,
507 e61170.

508 Spielmann, T., Gardiner, D.L., Beck, H.P., Trenholme, K.R., Kemp, D.J., 2006. Organization of
509 ETRAMPs and EXP-1 at the parasite-host cell interface of malaria parasites. Mol Microbiol 59, 779-
510 794.

511 Stack, C.M., Lowther, J., Cunningham, E., Donnelly, S., Gardiner, D.L., Trenholme, K.R., Skinner-
512 Adams, T.S., Teuscher, F., Grembecka, J., Mucha, A., Kafarski, P., Lua, L., Bell, A., Dalton, J.P.,
513 2007. Characterization of the *Plasmodium falciparum* M17 leucyl aminopeptidase. A protease involved
514 in amino acid regulation with potential for antimalarial drug development. J Biol Chem 282, 2069-
515 2080.

516 Tiburcio, M., Niang, M., Deplaine, G., Perrot, S., Bischoff, E., Ndour, P.A., Silvestrini, F., Khattab, A.,
517 Milon, G., David, P.H., Hardeman, M., Vernick, K.D., Sauerwein, R.W., Preiser, P.R., Mercereau-
518 Puijalon, O., Buffet, P., Alano, P., Lavazec, C., 2012. A switch in infected erythrocyte deformability at

519 the maturation and blood circulation of *Plasmodium falciparum* transmission stages. Blood 119, e172-
520 180.

521 Trager, W., Jensen, J.B., 1976. Human malaria parasites in continuous culture. Science 193, 673-675.

522 Watermeyer, J.M., Hale, V.L., Hackett, F., Clare, D.K., Cutts, E.E., Vakonakis, I., Fleck, R.A.,
523 Blackman, M.J., Saibil, H.R., 2016. A spiral scaffold underlies cytoadherent knobs in *Plasmodium*
524 *falciparum*-infected erythrocytes. Blood 127, 343-351.

525 Waters, S.P., Dalling, M.J., 1983. Purification and Characterization of an Iminopeptidase from the
526 Primary Leaf of Wheat (*Triticum aestivum L.*). Plant Physiol 73, 1048-1054.

527 World Health Organization, 2015. World Malaria Report, World Health Organization, Geneva

528 Wu, Y., Sifri, C.D., Lei, H.H., Su, X.Z., Wellems, T.E., 1995. Transfection of *Plasmodium falciparum*
529 within human red blood cells. Proc Natl Acad Sci U S A 92, 973-977.

530 Yoshimoto, T., Kabashima, T., Uchikawa, K., Inoue, T., Tanaka, N., Nakamura, K.T., Tsuru, M., Ito,
531 K., 1999. Crystal structure of prolyl aminopeptidase from *Serratia marcescens*. J Biochem 126, 559-
532 565.

533

534 **Figure Legends**

535 **Fig 1. A sequence alignment was used to construct a theoretical structural model of the catalytic**
536 **domain of *Pf*PAP.** A) ClustalX alignment of PF3D7_1401300 (N-terminal PEXEL region removed)
537 against the prolyl aminopeptidase from *S. marcescens* (UniProtKB 032449). Catalytic triad residues

538 (S249, D402, H430) are highlighted. B) Crystal structure of prolyl aminopeptidase from *S. marcescens*
539 (PDB code 1QTR). Catalytic residues are numbered and shown as Corey, Pauling, Koltun (CPK)
540 surfaces. The protein backbone is shown as a thin tube. C). Initial model structure of the putative prolyl
541 aminopeptidase PF3D7_1401300. Catalytic residues are numbered and shown as CPK surfaces. The
542 protein backbone is shown as a thin tube.
543
544 **Fig 2. Purification of a functionally active recombinant *Pf*PAP.** A). Purification of active r*Pf*PAP.
545 M, molecular size markers; S, soluble supernatant; W, washes; E, eluted r*Pf*PAP. Purified protein
546 migrates at ~45 kDa. B). Immunoblot confirmed identity of eluted purified r*Pf*PAP with primary mouse
547 anti-histidine antibody and secondary goat anti-mouse horseradish peroxidase antibody. C). Enzyme
548 assays with the fluorogenic peptide substrate H-Pro-NHMec demonstrate that the r*Pf*PAP exhibits
549 typical Michaelis-Menten enzymatic kinetics with a Km constant of 403.6 µM.
550
551 **Fig 3. *Pf*PAP is transcribed throughout the intraerythrocytic asexual lifecycle and exported into**
552 **the host RBC.** A). Northern blot analysis of PF3D7_1401300 transcription, RNA was probed with the
553 full length coding region of the gene. R = ring stage parasites. ET = early trophozoite parasites, LT =
554 late trophozoite parasites, S = schizont stage parasites. Analysis reveals transcription in all stages. B).
555 Quantitative analysis of *Pf*PAP transcription relative to reference genes demonstrates highest
556 transcription in early stages of the intra-erythrocytic asexual life cycle C). Western blot of 3D7
557 and 3D7_PAP-KO parasites probed with anti *Pf*PAP shows the loss of protein expression in the
558 knockout line. REX1 protein expression in both clones was used to demonstrate protein loading. C).
559 Direct fluorescence of transgenic parasites expressing PF3D7_1401300 C-terminally tagged with GFP.
560 BF = bight field, GFP = GFP fluorescence, Nuclei = nuclear staining with Hoechst, Merge = merge of
561 the previous images. Bar 5µm.

562

563 **Fig 4. Targeted gene disruption of *Pf*PAP changes the filterability of the infected RBCs but not**
564 **the expression or localization of KAHRP, REX1, and *Pf*EMP-3.** A). Analysis of filterability of
565 3D7_PAP-KO through micro beads designed to mimic the splenic microcirculation. Samples were
566 measured at 16, 18, 20 and 26 h post invasion. Data are presented as mean percentage of parasites
567 present in the flow-through relative to the starting parasitemia (± SEM; from 3 triplicate experiments).
568 B). Immunofluorescence using anti-KAHRP, REX1, and *Pf*EMP-3 antibodies on 3D7 and 3D7_PAP-
569 KO show no difference in the location of these proteins. C). Electron microscopy of 3D7_PAP-KO
570 showing electron dense structures at the surface of the infected erythrocyte indicative of the presence of
571 knobs. Bars are 5 μm.

572

573 **Fig 5. Targeted gene disruption of *Pf*PAP reduces CD36 cytoadhere under flow conditions** A).
574 Intact 3D7 and 3D7_PAP-KO infected RBCs were subjected to treatment with PBS (P) or trypsin (T)
575 or trypsin plus inhibitor (i), then extracted and subjected to SDS-PAGE and probed using an antibody
576 recognizing the ATS domain of *Pf*EMP-1. *Pf*EMP-1 cleavage products are indicated. B) 3D7 and
577 3D7_PAP-KO-infected RBCs adhere to recombinant CD36 at comparable levels under static
578 conditions C). 3D7_PAP-KO parasites have a reduced ability to cytoadhere to CD36 under flow
579 conditions. Adherence under flow conditions was assessed at flow rates equivalent to shear stresses of
580 0.1 and 0.05 Pa. The mean numbers (from 3 separate experiments) of parasites bound per mm^2 are
581 shown (± SEM).

582

A

```
PF140130      ----------CPYEYGEVFYGTHGIINYELKGNPESETLVITFHGLYGSNLEFYEIQKF
1QTR          MEQLRGLYPPLAAYDSGWLDTGDGHRIYWELSGNPNG-KPAVFIHGGPGGGISPHHRQLF
                        ..*: * :  *    * :**.***:. . .: :**  *..:. :. * *
PF140130      LVKSNYQVLNFDLYGYGLSATPKYNDKEKTYGVDFYVEQTEELLKHLNLENKDYYLMGES
1QTR          DPER-YKVLLFDQRGCGRSRPHASLDNNTTWHLVADIERLREMAG-----VEQWLVFGGS
                :  *:** **  * * * .    *::.*: :   :*: .*:        ::: ::* *
PF140130      MGCIIAAGFTRKITEKVKKMVLISPVGVLNEKP-WYLK------IFKKCSCLINLSTFVL
1QTR          WGSTLALAYAQTHPERVSEMVLRGIFTLRKQRLHWYYQDGASRFFPEKWERVLSILSDDE
               *. :* .::::.*.*:*.:*** . . : :::  ** :      : :* . ::.: :
PF140130      RPFCFRSFKGKMVNGYDDDEEVELDIGNGGNHNNSDDNDIYQKNE--FLYNRLMWHLFVK
1QTR          RKDVIAAYRQRLTS---ADPQVQLEAAKLWSVWEGETVTLLPSRESASFGEDDFALAFAR
              *   : ::: ::..    * :*:*: .:   .  :.:   :  ..*  : :  :   *.:
PF140130      KDNVAQSILGCINNLHMWSAHHIYREVGKIG-IPVLILGGKDDEYCSEEVFENTSRYFKN
1QTR          IENHYFTHLGFLE-----SDDQLLRNVPLIRHIPAVIVHGRYDMACQVQNAWDLAKAWPE
               :*   : ** ::     * .:: *:*  *  **.:*: *: *  *. :   : :: : :
PF140130      THLIIFDDASHLVLLEETRKINMCTLLFFK--
1QTR          AELHIVEGAGHSYDEPGILHQLMIATDRFAGK
              :.* *.::*.*       :  * :   *
```

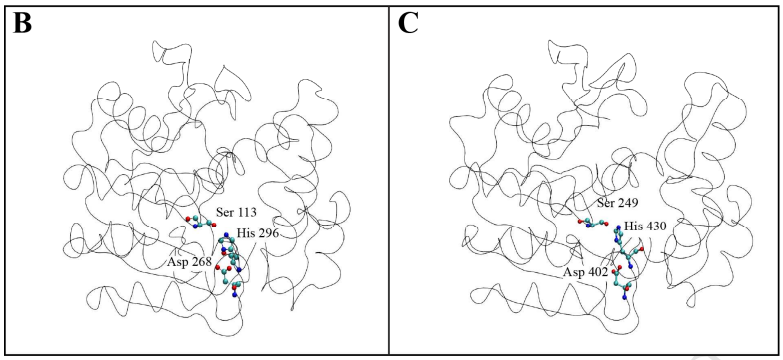

A **B**

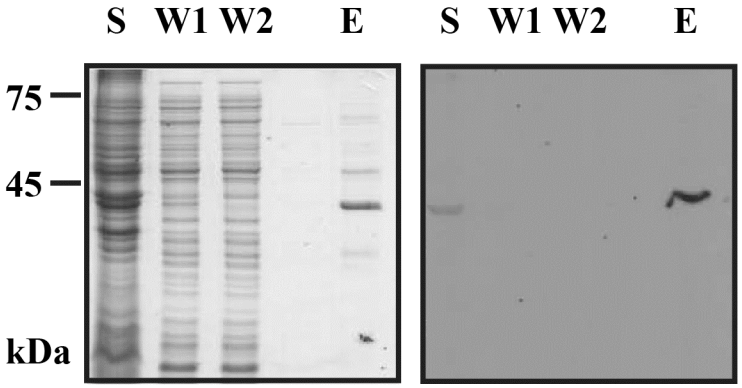

C

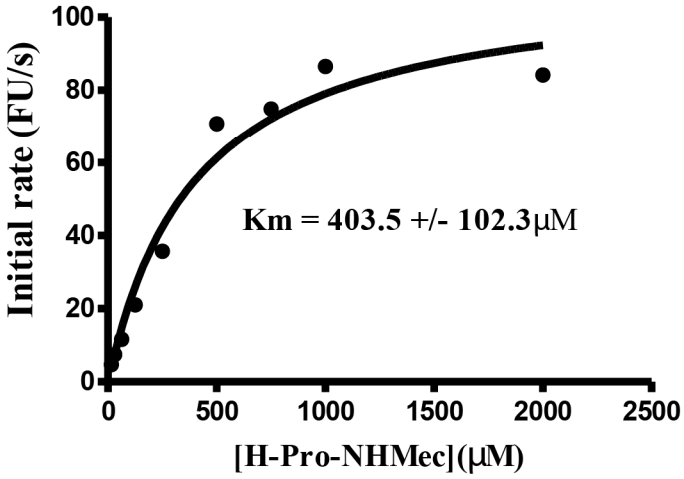

Substrate	H-Pro-NHMec
Kcat	0.0114 s-1 ± 0.0059
Km	403.5 ± 102.3µM
Kcat/Km	28.277 M-1s-1

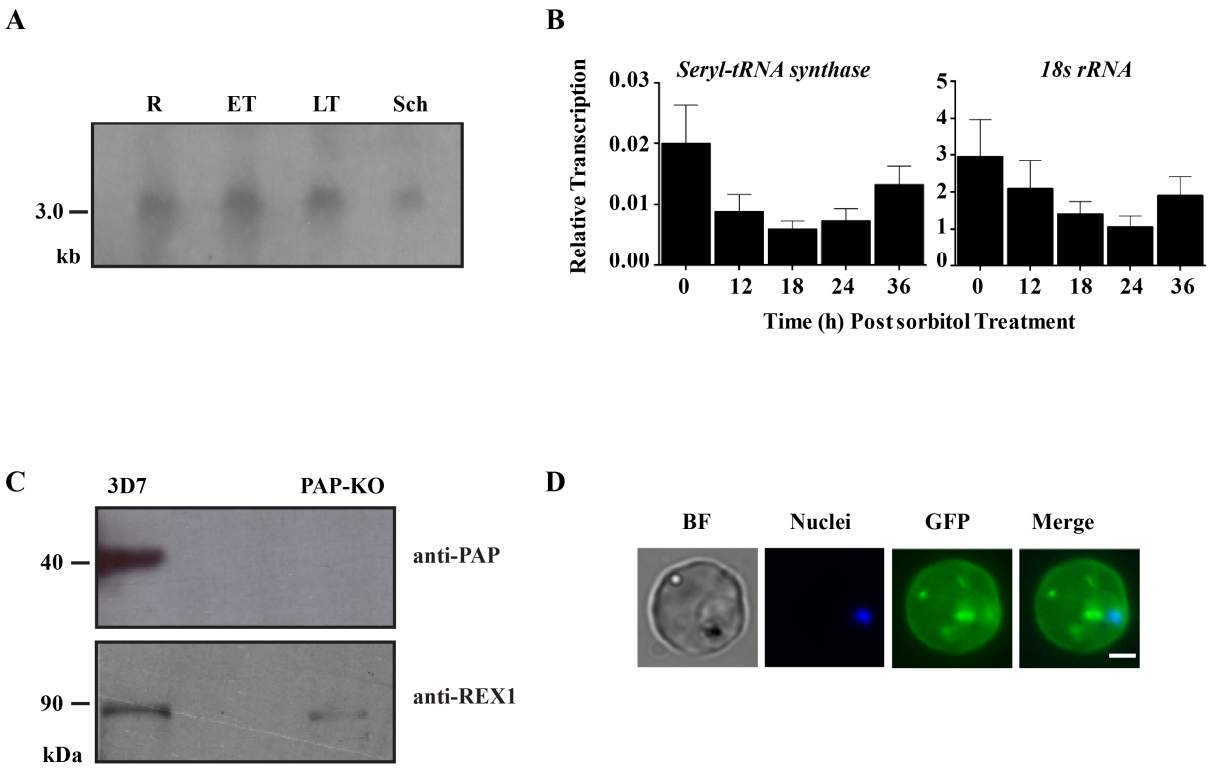

A

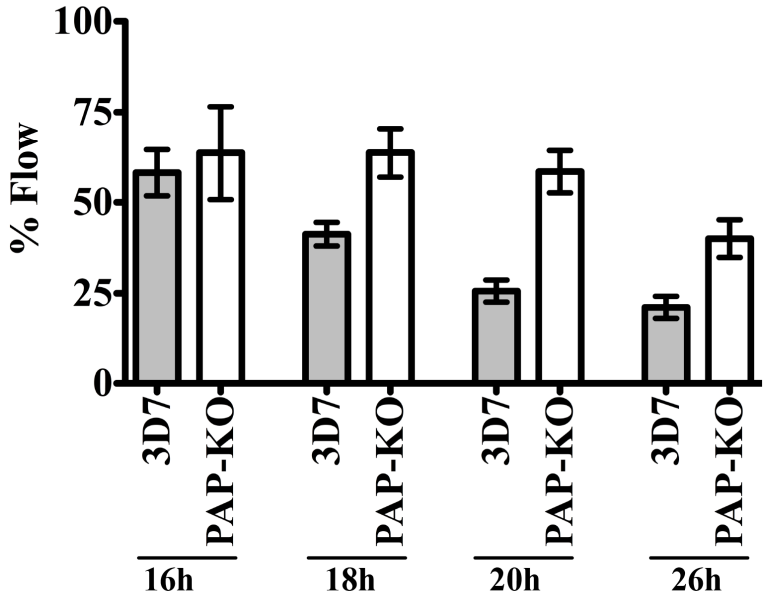
100
75
50
25
0
% Flow
3D7
PAP-KO
3D7
PAP-KO
3D7
PAP-KO
3D7
PAP-KO
16h
18h
20h
26h

B

i

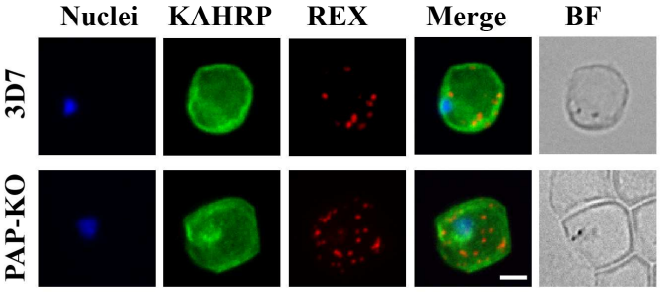
Nuclei
KΛHRP
REX
Merge
BF
3D7
PAP-KO

ii

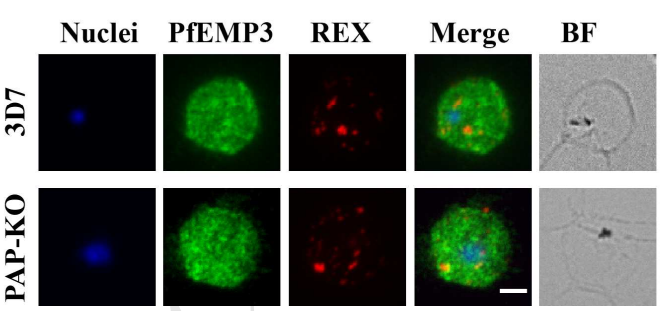
Nuclei
PfEMP3
REX
Merge
BF
3D7
PAP-KO

C

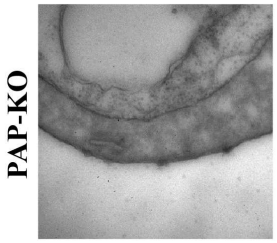
PAP-KO

A

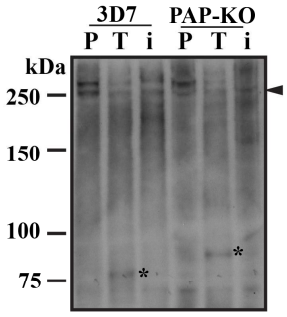

B

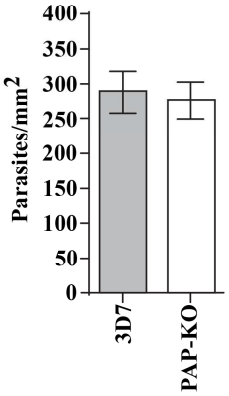

C

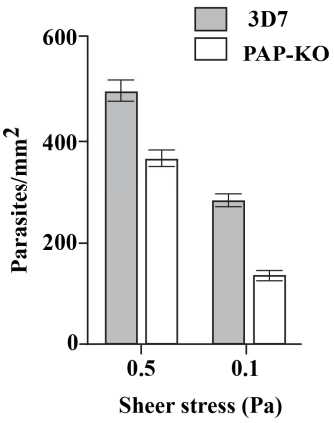

- The pathology of Falciparum malaria is associated with the remodelling of host RBCs
- We investigated the role of *Pf*PAP, a putative proline aminopeptidase in this process
- *Pf*PAP contains a predicted protein export element and is non-syntenic with other malaria species
- Our data confirm that *Pf*PAP is a proline aminopeptidase that it is exported into the host RBC
- Genetic deletion of *Pf*PAP suggests it plays a role in RBC rigidification and cytoadhesion